Oil slicks in the Gulf of Guinea - 10 years of Envisat ASAR observations

Zhour Najoui [a], Nellya Amoussou [c], Serge Riazanoff [a,b], Guillaume Aurel [a], Frédéric Frappart[d]

[a]*VisioTerra, 14 rue Albert Einstein Champs-sur-Marne, France, zhour.najoui-nafai@visioterra.fr,*

serge.riazanoff@visioterra.fr, guillaume.aurel@visioterra.fr.

[b]*Université Gustave Eiffel – Institut Gaspard Monge -IGM, 5 boulevard Descartes, Champs sur Marne, serge.riazanoff@univ-mlv.fr.*

[c]*Université de Sorbonne Université - Laboratoire d'Océanographie et du Climat : Expérimentations et Approches Numériques*

(LOCEAN), 4 Place Jussieu, 75005 Paris, lydieamoussou14@gmail.com

[d]*INRAE, ISPA, UMR 1391 INRAE/Bordeaux Sciences Agro, Villenave d'Ornon, France, frederic.frappart@inrae.fr*

Correspondence to: Zhour NAJOUI (zhour.najoui-nafai@visioterra.fr)

1. Abstract

Gulf of Guinea is a very active area regarding maritime traffic as well as oil and gas exploitation (platforms). As a result of some actors of both sectors that fail to comply with environmental standards, the region is subject to a large number of oil pollutions. This study aims to detect oil slicks spilled in the Gulf of Guinea and analyse their spatial distribution using Synthetic Aperture Radar (SAR) images. If previous works have already locally mapped oil slicks in this area, this study is the first one to achieve a global statistical analysis based on a very high number of radar images covering 17 Exclusive Economic Zones of the Gulf of Guinea. To carry out the present study, a database of 3,644 SAR images, collected between 2002 and 2012 by the Advanced SAR (ASAR) sensor onboard the European Spatial Agency (ESA) Envisat mission has been used. This database allowed the identification of 18,063 oil slicks (Najoui, 2022). These "Oil slicks" herein detected regroup: "oil spills" - of anthropogenic origin- and "oil seeps" - of natural origin (natural oil reservoir leaks).

2. Introduction

The Deep Water Horizon (DWH) disaster that occurred on April 20, 2010 in the Gulf of Mexico aroused worldwide outrage both for its human and environmental impacts (Leifer et al., 2012). There was great interest of the public, media, politicians and scientists characterized by a meticulous follow-up of the progression of the oil slicks (Caruso et al., 2013; Pinkston and Flemings, 2019). And yet, a disaster similar to that of the DWH would not be surprising along the African coast and in particular in the Gulf of Guinea where recurrent oil spills are observed. These may be caused by deballasting operations (Albakjaji, 2010) and releases due to shipwrecks (Fuhrer, 2012).

If oil constitutes an important economic resource for the countries of the Gulf of Guinea from an economic point of view (Ovadia, 2016), the environmental impact caused by the frequent oil spills provokes serious negative effects on both the environment and the local economy (Jafarzadeh et al., 2021; Okafor-Yarwood, 2018; Yaghmour et al., 2022). The weakness of national monitoring and legislation control is likely to limit the compliance to the major standards followed by large companies. Thus, the provision of observation tools that can enable people of Africa to ensure good monitoring and better management of the Gulf of Guinea is necessary.

Synthetic Aperture Radar (SAR) images have proven to be a useful tool for oil slicks mapping due to the dampening effect that oil has

31 on capillary and small gravity waves, called Bragg waves. The latter are generated on water by local winds and they are responsible for the

32 radar backscattering (Gade et al., 1998; Jackson et al., 2004; Mercier and Girard-Ardhuin, 2006; Shu et al., 2010; Xu et al., 2015). As a

33 consequence, oil slicks appear darker compared nearby undampened water surface where Bragg waves produce brighter radar backscattering.

34 In addition, historical radar images are freely available since 1991 (ERS-1 mission was launched in 1991, ERS-2 in 1995, Envisat in 2002,

35 Sentinel-1a in 2014 and Sentinel-1b in 2016) while near real time radar images are foreseen to be freely available at least until 2030 owing to

36 Sentinel constellation. This availability of data allows extensive studies of past and future pollutions as well as operational detection of oil

37 slicks using satellite radar imagery (Kubat et al., 1998).

38 In this study, the European Spatial Agency (ESA) mission Envisat has been used. Envisat, the second generation of SAR satellite

39 developed by ESA, was launched on March 1, 2002 and had on board ten widely instruments (Louet and Bruzzi, 1999)). The Advanced

40 Synthetic Aperture Radar (ASAR) used in this study is one of these instruments. Its nominal life (5 years) has been doubled until the loss of

41 the satellite on April 8, 2012 (10 years).

42 The Gulf of Guinea is now one of the largest oil producing regions of the world, yet very few studies have really analysed its situation

43 regarding oil slicks (both spills and seeps). The studies that have been carried out so far are limited to very specific Exclusive Economic

44 Zones. This is the case with the studies by Jatiault et al. (2017) in the Congo Basin. The present study focuses on the spatial distribution of

45 the oil slicks occurring from 2002 to 2012 by Exclusive Economic Zone (EEZ) throughout the Gulf of Guinea using Envisat ASAR radar

46 images.

3. Presentation of the study area

3.1. Geographic location

49 The radar images used for this study were acquired over the Gulf of Guinea. This region is located in the Atlantic Ocean in the southwest

50 of Africa. According to the International Hydrographic Organization (Bassou, 2016), it extends from Guinea Bissau to Angola. It covers the

51 EEZs of 16 countries bordering the coast (extending over 7000 km): Guinea Bissau (GNB), Guinea Conakry (GIN), Sierra Leone (SLE),

52 Liberia (LBR), Ivory Coast (CIV), Ghana (GHA), Togo (TGO), Benin (BEN), Nigeria (NGA), Cameroon (CMR), Equatorial Guinea (GNQ),

53 Sao Tome and Principe (STP), Gabon (GAB), Republic of Congo (COG), Democratic Republic of Congo (COD), and Angola (AGO)

54 (fig. 1).
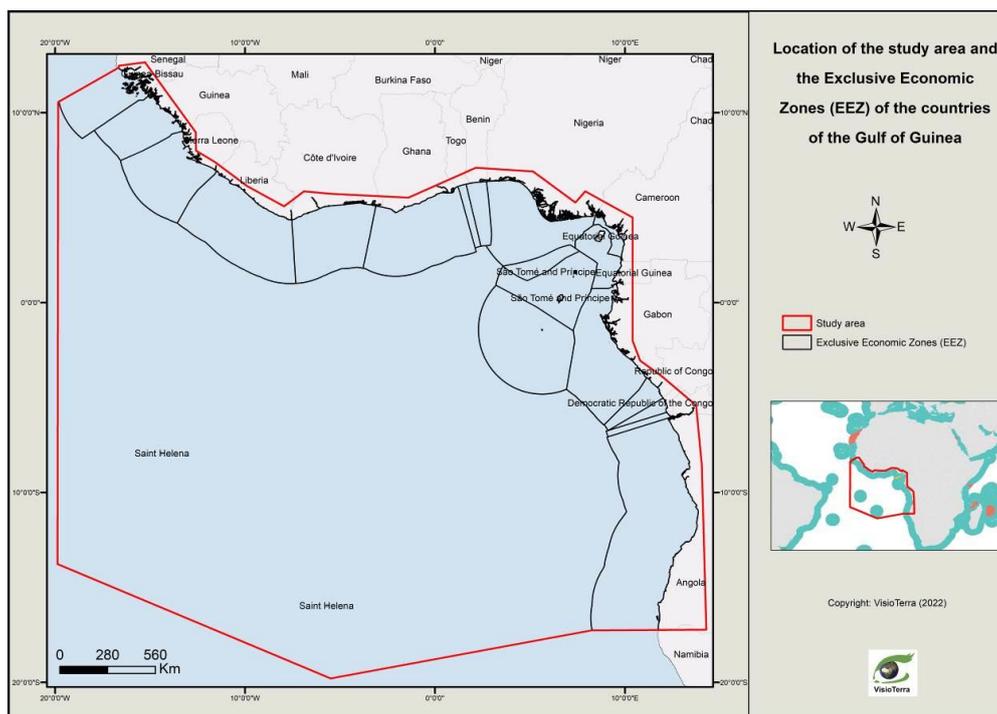
fig. 1 - Location of the study area in the Gulf of Guinea and the Exclusive Economic Zones of the different countries.

3.2. Geological location

Petroleum is a natural mixture composed mainly of hydrocarbons. It is formed within certain sedimentary rocks by transformation of organic matter (plankton, plants, animals, etc.) which is incorporated into the deposit. It is a slow and gradual process occurring in a sedimentary basin.

Indeed, the transformation of organic matter into oil spans millions of years, and is punctuated by several stages including the formation of an intermediate substance called kerogen. A given layer of sediment sinks and is buried under other layers of sediment. Depending on the filling of the basin, the heat flow and pressure induced by geologic processes, organic matter may change from kerogen to petroleum. Oil being less dense than water, it tends to migrate to the upper layers of the sedimentary strata. These sedimentary strata have a certain geometric configuration defined by the tectonic structure of the basin. During this structuring, different areas may have risen higher (anticlines) or sunk lower (synclines) relatively to the rest of the stratum. When these upper zones are topped by a cover allowing the oil to escape through faults or fractures, they constitute oil deposits exploited nowadays in offshore or onshore areas.

The Gulf of Guinea is located in a passive zone resulting from the opening of the South Atlantic Ocean initiated during the Lower Cretaceous, breaking up south-west Gondwana. The climate during this period was hot, humid and stable, which favours chemical weathering of the mainland. Eroded material brought chemical elements to the Gulf of Guinea; in particular, the Niger Delta transported sediments rich in hydrocarbons. These numerous characteristics make this area a source of natural seepages also called oil seeps (Lawrence et al., 2002)

24

3.3. Oil exploration in the Gulf of Guinea

73

74 The Gulf of Guinea region has entered the global oil landscape comparatively quite recently. In 1982, the signing of the Montego Bay

75 convention extended the maritime territories of riparian countries over their EEZ, 200 nautical miles off their coast, which encouraged

76 offshore exploration (Bassou 2016). The Gulf of Guinea is now one of the largest oil producing regions in the world.

77 Indeed, since the installation of its first oil platforms (anchored and floating platforms) between 1960 and 1970 (Favennec et al., 2003),

78 the Gulf of Guinea has become one of the favourite destinations of international oil investors (Tull, 2008). The good quality of its oil justifies

79 the attractiveness of foreign countries to the region (Ngodi, 2005). Since the 2000s, it has supplied more than 55 billion barrels, i.e. 5% of

80 world oil production (Mfewou et al., 2018) and 60% of total daily crude oil production in sub-Saharan Africa. Offshore is the default mode

81 of oil extraction in the Gulf of Guinea (Favennec et al., 2003). The depletion of coastal water resources (shallow water; ≤ 200 m) means that

82 the relative share of deep water exploration (Deep water; 450 m - 1800 m), or even in ultra-deep water (1800 m - 3000 m) is increasing. This

83 is the case, for example, off the coast of Gabon.

3.4. Oil pollution and environmental impacts

84

85 The Gulf of Guinea is a very active area in oil exploration. The oil spills found there are unparalleled in frequency and their toxicity

86 induces serious repercussions both on the marine environment and on the ecosystem (Bagby et al., 2017; Chalghmi, 2015; Khanna et al.,

87 2018; Langangen et al., 2017; Li et al., 2019; Li and Johnson, 2019; NAE-NRC, 2012; Reuscher et al., 2020).

88 Several cases of accidents caused by the exploitation of offshore oil are documented. Apart from these cases, several accidents have

89 occurred following the exploitation of offshore oil fields. The frequency of oil spills in the Gulf of Guinea is said to be due, among other

90 things: to oil production operations, inadequate production equipment leading to corrosion of pipelines and tanks, to disasters, sabotage and

91 vandalism (Adelana and Adeosun, 2011).

92 Environmental consequences include the loss of habitat for corals and seagrass, the destruction of flora (reduction of mangroves and

93 certain species of algae) and that fauna (extinction of sea turtles) (Scheren et al., 2002).

4. Dataset and Method

94

4.1. Radar data

95

96 Several spaceborne SAR systems have been widely used for marine pollution monitoring and mapping (Brekke and Solberg, 2008; Del

97 Frate et al., 2000; Espedal, 1999; Fiscella et al., 2000; Gade et al., 1998; Garcia-Pineda et al., 2008; Kanaa et al., 2003; Li and Johnson,

98 2019; Liu et al., 1997; Marghany, 2015; Solberg et al., 1999). In this study, we used SAR images acquired by Envisat ASAR (Advanced

99 Synthetic Aperture Radar), an ESA mission that lasted from 2002 to 2012. Envisat ASAR operated in C-Band (4.20 – 5.75 GHz) in a variety

100 of modes including WSM (Wide Swath Medium-resolution) that acquired a 400 km by 400 km wide swath image. Its spatial resolution was

101 approximately 150 m by 150 m with a pixel spacing of 75 m by 75 m. It functioned in one of two polarizations types, either HH or VV.

102 ASAR. WSM operated according to the ScanSAR principle, using five predetermined overlapping antenna beams which covered the wide

103 swath. The ScanSAR principle consists in achieving swath widening by the use of an antenna beam which is electronically steerable in

104 elevation (Miranda et al., 2013).

105   On a radar image, the areas covered by oil appear smooth dark regions with low backscattering. This is due to the damping effect that the

106   oil produces on capillary waves and small waves of gravity. On a free-oil surface, a significant part of the energy will be backscattered

107   towards the radar making it appear lighter (Alpers et al., 2017). The backscatter of the radar signal is also influenced by environmental

108   conditions which are: wind speed and sea state (Fingas and Brown, 2017; Zhang et al., 2014). The ideal wind speed for the detection of oil

109   slicks is in an interval that depends on the authors: - 2 m/s to 10 m/s (MacDonald et al., 2015), - 1.5 m/s to 6.5 m/s (Jatiault et al.,

110   2017), - 2.09 m/s to 8.33 m/s (Najoui, 2017)... Vertical polarization (VV) is the most effective mode for detecting oil spills on the sea surface

111   (Brekke and Solberg, 2008; Jatiault et al., 2017; Najoui et al., 2018a, 2018b).
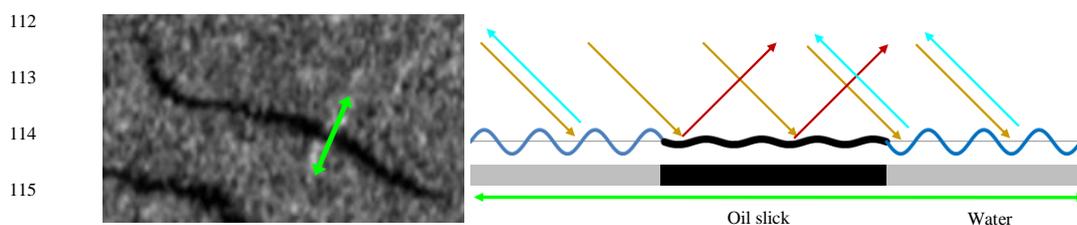
117   *fig. 2 - Backscattering of the radar signal in the presence and absence of oil (Najoui, 2017).*

118   An amount of **3,644** Envisat ASAR WSM images produced and distributed by the European Spatial Agency have been processed over

119   the study area. The fig. 3 illustrates the spatial distribution of the occurrences of Envisat ASAR WSM observations between 2002 and 2012

120   in the Gulf of Guinea. The number of WSM observations is noticeably higher near the coasts.
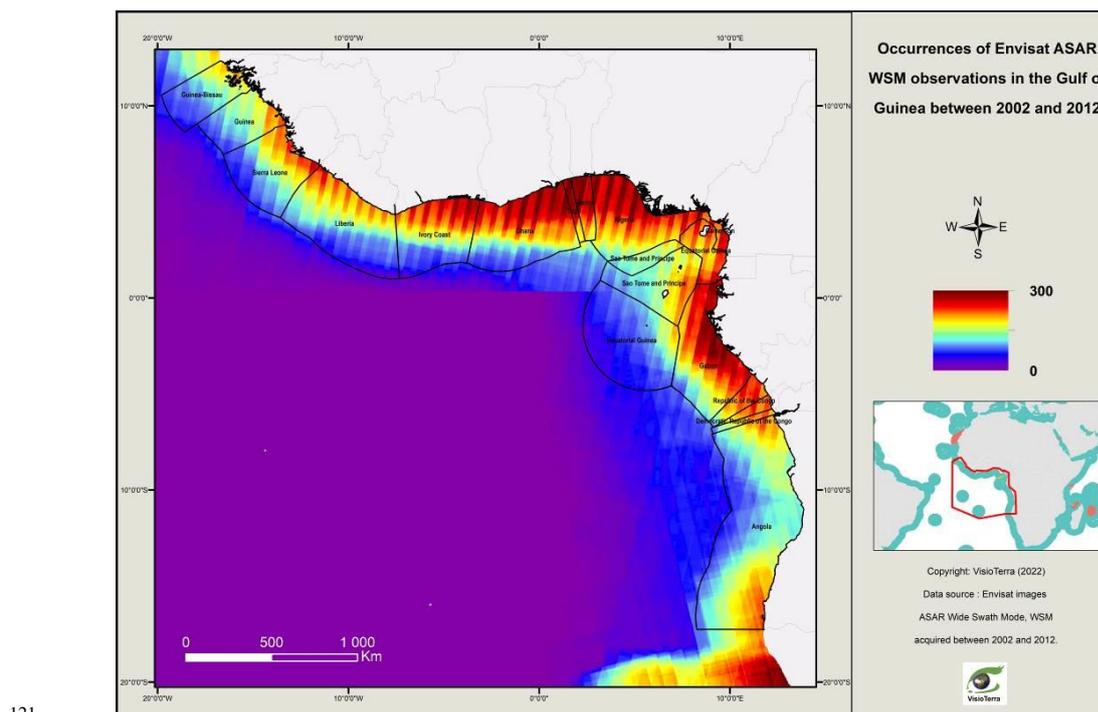
122   *fig. 3 - Occurrences of Envisat ASAR WSM observations between 2002 and 2012.*

²6

4.2. Image preprocessing

The database of 3,644 images has been georeferenced in the geographic coordinate reference system over the WGS84 ellipsoid, datum WGS84. A land mask has been applied and the images have been radiometrically corrected. The radiometric correction consists in correcting the brightness variations due to SAR peculiarities. Indeed, the radar backscattering on the offshore area is dominated by non-Lambertian reflections (the surface does not reflect the radiation uniformly in all directions). This non-Lambertian reflection leads to heterogeneity of the brightness in the radar image. The input images have a 16-bits Digital Number (DN) dynamic which requires reduction to 8-bits to be displayable on an usual screen. The applied preprocessing consists in applying a local stretching with an average of 140 and a standard deviation of 60 on a sliding window of 301 pixels in order to optimize the detectability of the oil slicks (fig. 4) (Najoui, 2017; Najoui et al., 2018b).
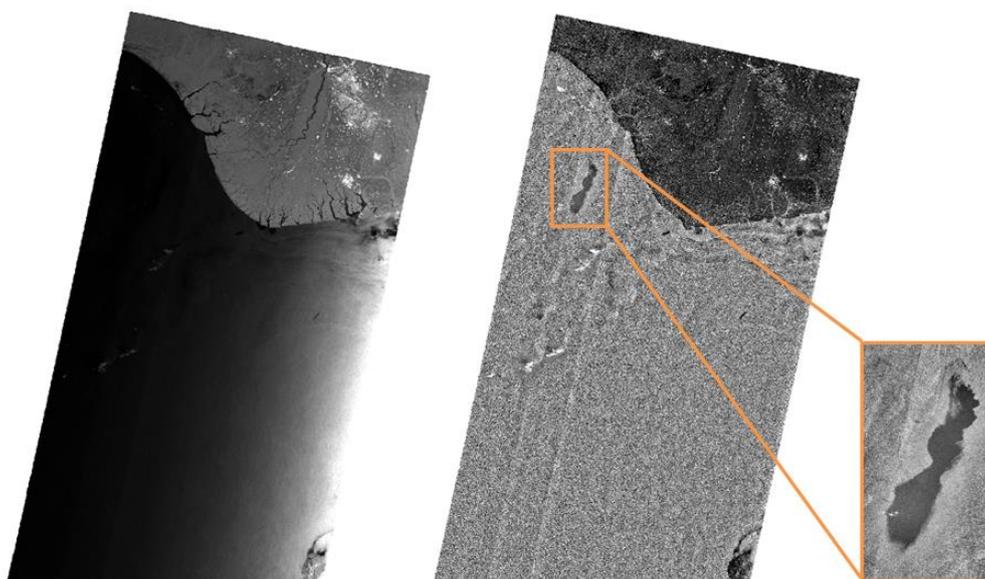
fig. 4 - ASAR WSM images before (left) and after (right) local stretching showing a leak from an oil platform.

4.3. Manual detection

Oil slicks appear as dark patches on radar images because they flatten the surface of the sea. However, in addition to oil slicks, many phenomena also may appear as dark. Non-oil dark patches are termed as look-alikes features that include upwelling, eddies, rainfalls, wind shadows, bathymetry, internal waves, current shear zones, etc. (Brekke and Solberg, 2005; Espedal, 1999; Xu et al., 2015).

The detection of oil slicks has been performed using a reliable manual detection approach as explained in (Najoui et al., 2018a, Jackson et al., 2004). In fact, the 3,644 radar images used in this publication have been manually interpreted. Therefore, the detected oil slicks have been categorized according to the interpretation based on morphological and textural criteria. Oil slicks may be subdivided into two major classes: biogenic and mineral. Biogenic oil slicks are organic films made of substances produced by plankton and other marine organisms. The mineral oil slicks can be subdivided between natural seeps emitted naturally from the sea bottom and anthropogenic oil spills that originate from ships, refineries, oil terminals, industrial plants, oil platforms and pipelines (Espedal, 1999). For instance, oil spills from

144 platforms or ships induce significant slicks (Johannessen et al., 2000; Leifer et al., 2012; Trivero and Biamino, 2010). If biogenic oil slicks

145 appear as shiny diffracting points on SAR data, oil seeps are characterized by curvilinear shapes due to short-term changes of the strength

146 and orientation of the wind and of the surface currents (Espedal, 1999). Thereafter, a multi-date analysis has been performed. We use all the

147 interpretations at different dates in order to assess the manual interpretation. Indeed, repetitive slicks are more likely due to leaks from static

148 sources: a geological feature for oil seeps, a platform or pipeline for oil spills, for instance. The shape of these oil slicks from static sources is

149 induced by the strength and orientation of the short-term changes of both wind and sea surface current. Usually, this type of slicks from

150 natural oil seeps and oil spill from oil platforms constitutes forms of "astroseeps" or "flower structures". In general, ships that discharge oily

151 effluents do it in route, leaving behind the ship linear-shaped spills or trails. When oil is discharged in a current-free and calm sea, the

152 resulting overall spill geometry will follow the route of the ship. This linearity is used to identify such oil spills. However, when a

153 deballasting ship maneuvers or when a non-uniform surface current is present, then the contour of the spill can deviate significantly from

154 linearity. When oil is discharged from a moving ship, it also spreads laterally, resulting in oil trail which width increases with distance from

155 the ship.

156 The validation of our analysis has been performed by the integration of the manual detection output in a Geographic Information System

157 with other auxiliary data. This work led to the constitution of a dataset with 18,063 interpreted oil slicks (Najoui, 2022).

158 ***4.4. Mean area covered in oil***

159 The photo-interpretation described in the previous section results in the delimitation of closed polygons corresponding to the slicks.

160 These polygons are "embedded" in a raster image to perform the statistical study. Because each location within the area of interest has not

161 been imaged an equal number of times by the Envisat satellite, an observation occurrence map has been produced (fig. 3). In fact, each

162 location has not been equally observed because of the partial overlap of neighbouring swaths and the use of both ascending and descending

163 orbits. Hence, it was necessary to locally normalize the oil slicks number distribution by dividing the number of oil slick occurrences by the

164 number of observations made by Envisat ASAR over the study area. This gives relative frequency of the presence of oil per pixel.

165 The **probability of presence of oil X per pixel ($P_X(l,p)$)** is equal to the number of occurrences of oil X in a pixel ($S_X(l,p)$) divided by the

166 number of observations ($O(l,p)$) of the same pixel (eq.1).

$$P_X(l,p) = \frac{S_X(l,p)}{O(l,p)}$$

(eq. 1)

167 Where :

168
169 • $S_X(l,p)$ is the number of occurrences of the presence of oil X detected on a pixel by photo-interpretation,

170
171 • X is the type of oil. It can be natural leaks (oil seepages), pollution by boats (oil spill ships) and pollution by platforms (oil spill platforms),

172 • (l,p) are the coordinates (l, p) of the current pixel representing the rows and columns of the image,

173
174 • O(l,p) are the number of observations as they appear in the footprints of the processed images Envisat ASAR WSM,

175 • $P_X(l,p)$ is the normalized occurrence also called probability of oil presence at pixel (l, p).

176 For each class X of oil slick among (s) "seepage", (s) "spill from ship", and (p) "spill from platform", the generic definition given in

177 (eq.1) becomes the ones given in (eq.2).

28

$$P_e(l,p) = \frac{S_e(l,p)}{O(l,p)} \; , \; P_s(l,p) = \frac{S_s(l,p)}{O(l,p)} \; , \; P_p(l,p) = \frac{S_p(l,p)}{O(l,p)} \qquad (\text{eq. 2})$$

178   Where :

179   • $S_e(l,p)$, $S_s(l,p)$ et $S_p(l,p)$ are the number of occurrences of oil presence detected on a pixel by photo-interpretation of
180   natural leaks (oil seepages), pollution of boats (oil spill ships) and pollution of platforms (oil
181   spill platforms) respectively,

182   • (l,p) are the coordinates (l, p) of the current pixel representing the rows and columns of the image,

183   • $O(l,p)$ are the number of observation as they appear in the footprints of the processed images Envisat
184   ASAR WSM,

185   The total probability of presence of oil X per pixel ($P_t(l,p)$) is equal to:

$$P_t(l,p) = \frac{S_e(l,p)}{O(l,p)} + \frac{S_s(l,p)}{O(l,p)} + \frac{S_p(l,p)}{O(l,p)} \qquad (\text{eq. 3})$$

186   Thus, we denote by $\hat{A}_X$ the mean area covered in oil of origin X in the Gulf of Guinea between 2002 and 2012. This mean area is given

187   by (eq.4).

$$A_X = \sum_{GG}^{l} \sum_{GG}^{p} (P_X(l,p) \times A(l,p)) \approx \sum_{GG}^{l} \sum_{GG}^{p} (P_X(l,p)) \times \overline{A} \qquad (\text{eq. 4})$$

188   Where:

189   • $A(l,p)$ is the area of the pixel (l,p),

190   • $\overline{A}$ is the mean area of a pixel. The variation of the area of the pixel (75 m x 75 m) is less than
191   2.5 % over the Gulf of Guinea.

192   For a given year Y, the mean area covered in oil of origin X ($\hat{A}_{X,Y}$) is given by (eq.5).

$$A_{X,Y} = \sum_{GG}^{l} \sum_{GG}^{p} (P_{X,Y}(l,p)) \times \overline{A} \qquad (\text{eq. 5})$$

193   Where:

194   • $P_{X,Y}(l,p)$ is the probability of presence of oil of origin X for a given year Y for a given pixel (l,p).

195   For a given year Y and for a given EEZ, the mean area covered in oil of origin X ($\hat{A}_{X,Y,EEZ}$) is given by (eq.6).

$$A_{X,Y,EEZ} = \sum_{EEZ}^{l} \sum_{EEZ}^{p} (P_{X,Y}(l,p)) \times \overline{A} \qquad (\text{eq. 6})$$

196   *4.5. Mean fraction covered by oil for a given EEZ*

197   For each country's EEZ over a given period of time, we estimated the mean fraction covered in oil of origin X and for a given year Y

198 ($P_{X,Y,EEZ}$) by dividing the mean area covered in oil of origin X for a given year Y for a given EEZ ($\hat{A}_{X,Y,EEZ}$) by the area of the country's

199 EEZ A_{EEZ} (eq.7). When presenting the results, the term EEZ was replaced by the country's ISO code.

$$P_{X,Y,EEZ} = \frac{A_{X,Y,EEZ}}{A_{EEZ}}$$

(eq. 7)

200 5. Results and discussion

201 **5.1. Spatial distribution of oil slicks in the Gulf of Guinea**

202 The spatial and temporal analysis on the Gulf of Guinea allowed the photo-interpretation of 18,063 oil slicks. The database of the 18,063

203 identified objects includes two classes of mineral oil. On the one hand, anthropogenic pollution that come from oil spill platforms and

204 recurring deballasting of oil spill ships. On the other hand, natural oil seepage resurgences which are hints of the presence of hydrocarbon

205 reservoirs in the sub-surface of the Gulf of Guinea. The fig. 5 represents the "hyperlook" of an oil spill platform encountered near the

206 Nigerian coasts.
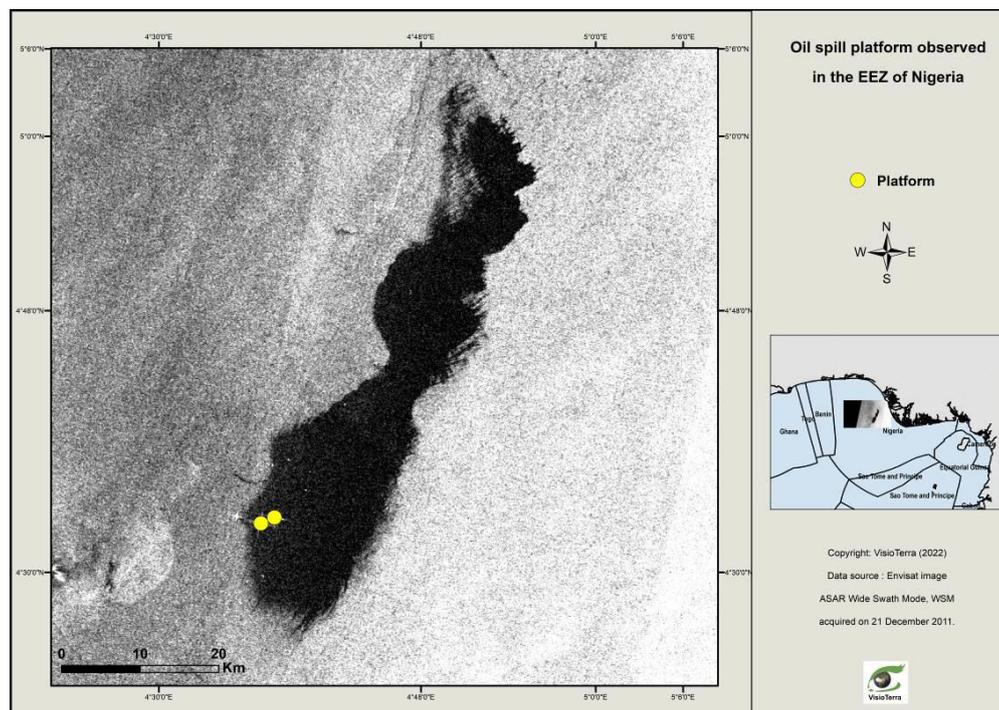
207

208 *fig. 5 - Oil spill platform observed in the EEZ of Nigeria. The platforms are represented by the yellow dots*
209 *http://visioterra.org/VtWeb/hyperlook/504c7208cc184c12b42ed036bc9912f3.*

210 The fig. 6 illustrates the spatial distribution of the 18,063 oil slicks that have been detected and then mapped in the Gulf of Guinea over

211 the period 2002-2012. The fig. 7, fig. 8, and fig. 9 respectively show the density maps of oil seepages, spill form ships and spill from

212 platforms.
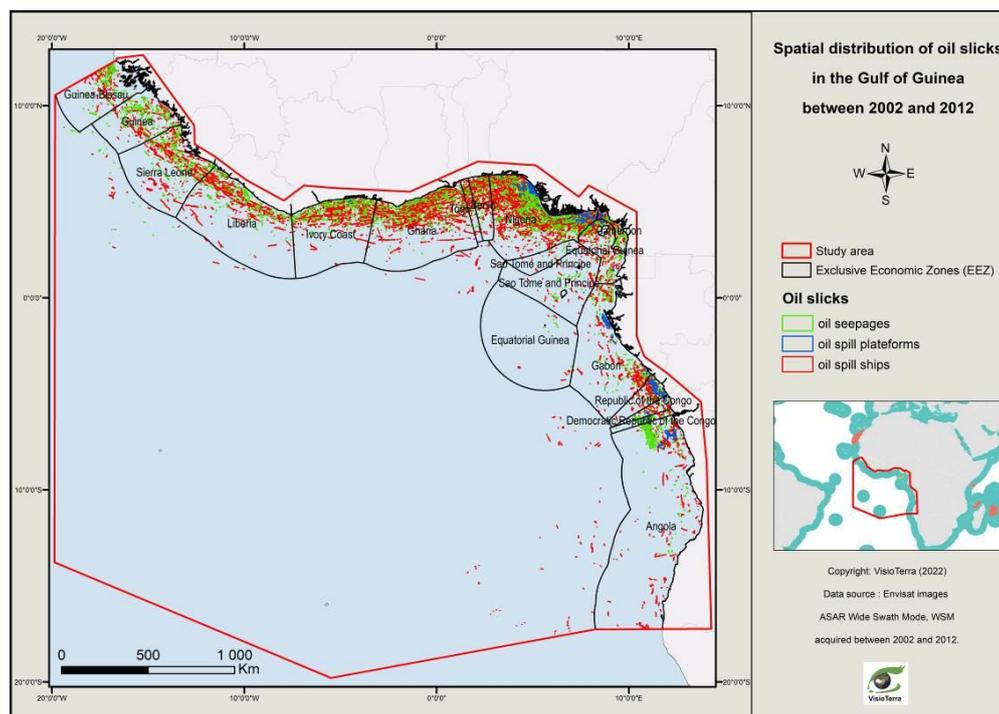
fig. 6 - Spatial distribution of oil slicks in the Gulf of Guinea between 2002 and 2012.

215   The fig. 7 shows that oil seepages are distributed over all the EEZs in the Gulf of Guinea. This large amount of oil seepages from the

216   Gulf of Guinea could be partly explained by its geology resulting from the opening of the South Atlantic domain initiated in the Lower

217   Cretaceous and by the significant sediment supply from the Niger Delta.

218   The proximity of the main maritime routes to the coasts contributes to the concentration of discharges in these places. This phenomenon

219   is especially noticed along the coasts of Nigeria which is one of the main shipping routes and occupies a place in maritime piracy (see fig. 8).

220   Thus, there are significant spills of ships there, despite the international convention for the prevention of pollution from ships (MARPOL

221   73/78), which came into force in 1983. Illegal dumping operations include deballasting and cleaning of ship engines.

222   Offshore oil platforms have been found all along the coasts of the EEZs of the top oil producing countries (Nigeria, Angola, Republic of

223   Congo, Ghana...) in the Gulf of Guinea (see fig. 9). The oil spills coming from platforms that have been observed in our study are very well

224   correlated with offshore installations.

225
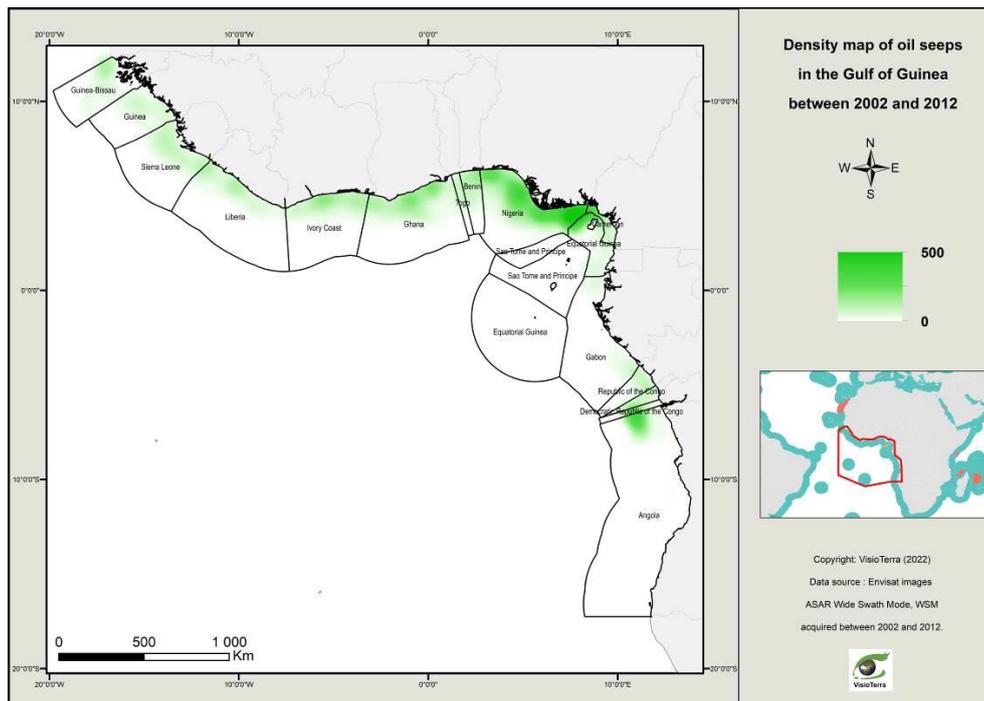
226   *fig. 7 - Density map of oil seeps in the Gulf of Guinea between 2002 and 2012.*
227
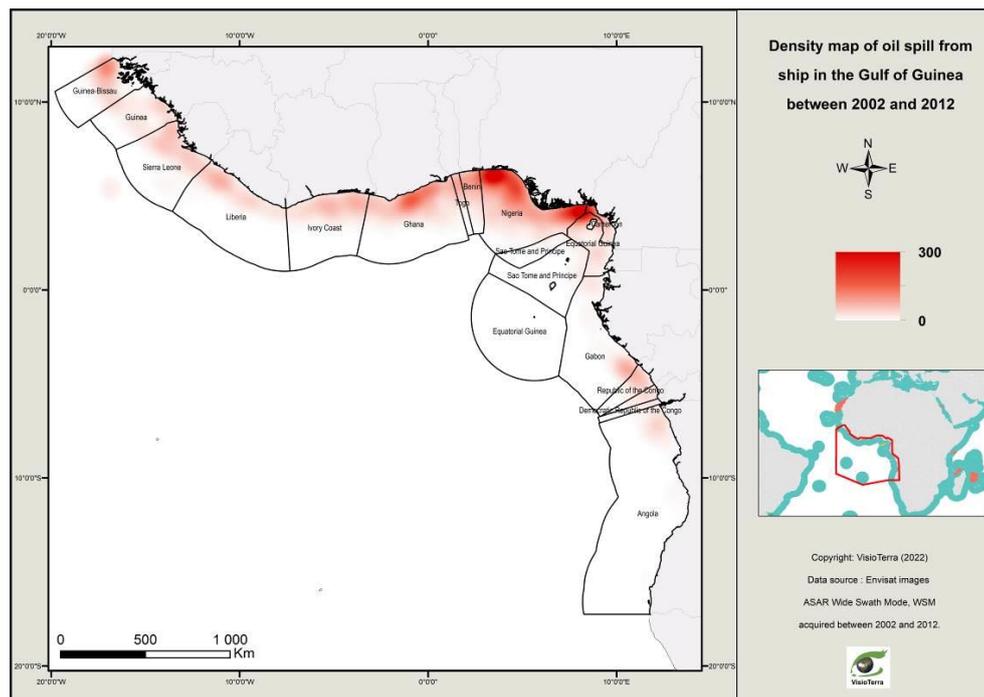
228

229   *fig. 8 - Density map of oil spill from ship in the Gulf of Guinea between 2002 and 2012.*

230
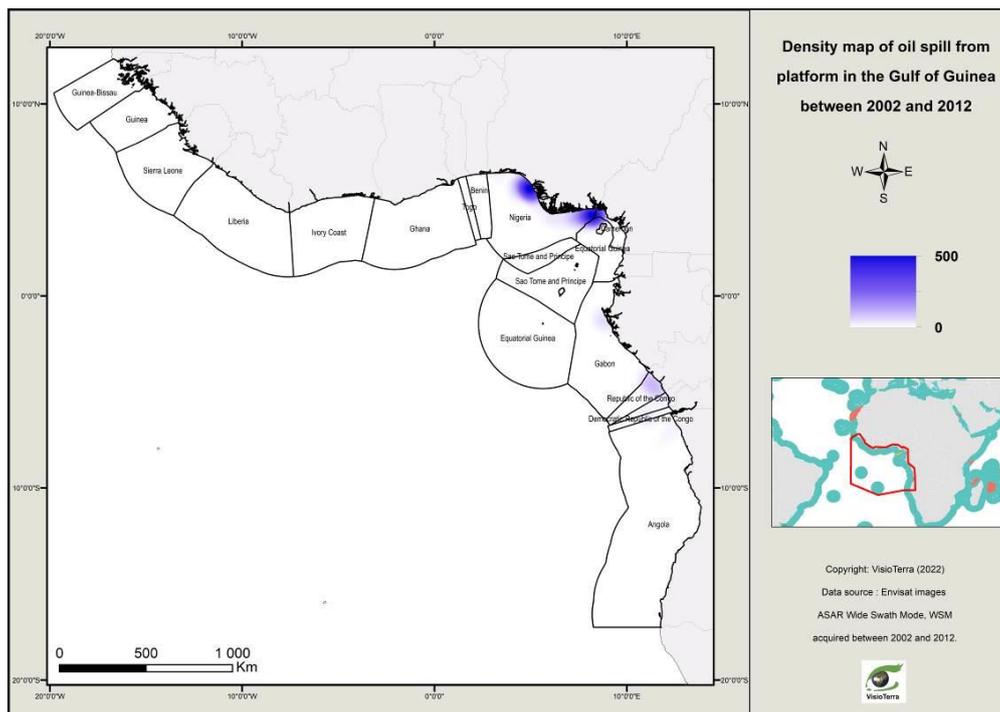
231

232   *fig. 9 - Density map of oil spill from platform in the Gulf of Guinea between 2002 and 2012.*

233   **5.2. Mean area covered in oil ($\hat{A}_{X,Y,EEZ}$)**

234   5.2.1. Mean area covered in oil in the Gulf of Guinea ($\hat{A}_{X,Y}$)

235   The fig. 10 shows the mean area covered in oil in the Gulf of Guinea by year. One can notice that:

236   • the mean area covered in oil slicks from natural origin (oil seeps) remains more or less stable during the period 2002-
237   2012,

238   • the mean area covered with oil slicks from oil spill platforms seems to have increased significantly during 2008 and
239   then returned to normal in 2009 until the end of the study period,

240   • the mean area covered in oil slicks from ships seems to have increased after 2004 with a peak between 2007 and 2008,
241   then have fallen in 2009 and remained stable until the end of the study period.
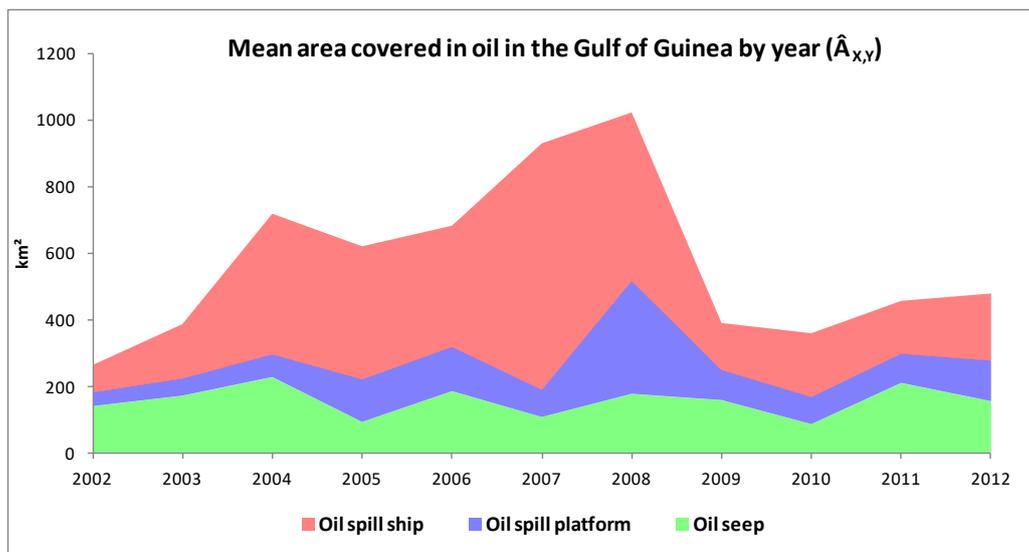
243 *fig. 10 - Mean area covered in oil in the Gulf of Guinea by year ($\hat{A}_{X,Y}$).*

244 5.2.2. Mean area covered in oil by EEZ of country ($\hat{A}_{X,Y,EEZ}$)

245 The fig. 11 shows the mean area covered in oil by EEZ of countries between 2002 and 2012. The fig. 12 shows the mean area covered in

246 oil by EEZ of countries by year. One may note that the most polluted EEZ are Nigeria followed by Angola, Republic of Congo and

247 Cameroon.

248 The analysis by EEZ shows that the decrease in oil spills observed between 2008 and 2009 (fig. 10) is governed by the major oil

249 producing countries: Angola, Nigeria and Republic of Congo (fig. 12).

250 The fall in the mean area covered in oil from platforms and ships may be explained by the economic crisis of 2008. In fact, 2008 world crisis

251 had led to the falling oil prices inducing deficit in the budget of oil companies and governments. For instance, Angola oil production

252 decreased in 2009 following the post-2008 slowdown in global economic activity and the subsequent glut of oil on the global market

253 (Mikidadu, 2018).

²14
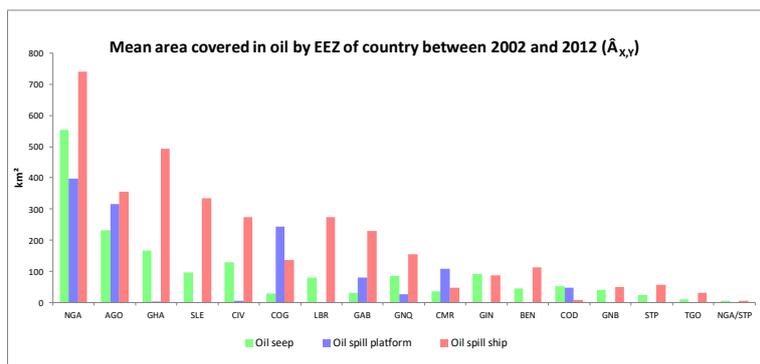
254

255   *fig. 11 - Mean area covered in oil by EEZ of country (Â$_{X,Y}$) between 2002 and 2012.*

256

257

258

259

260

261
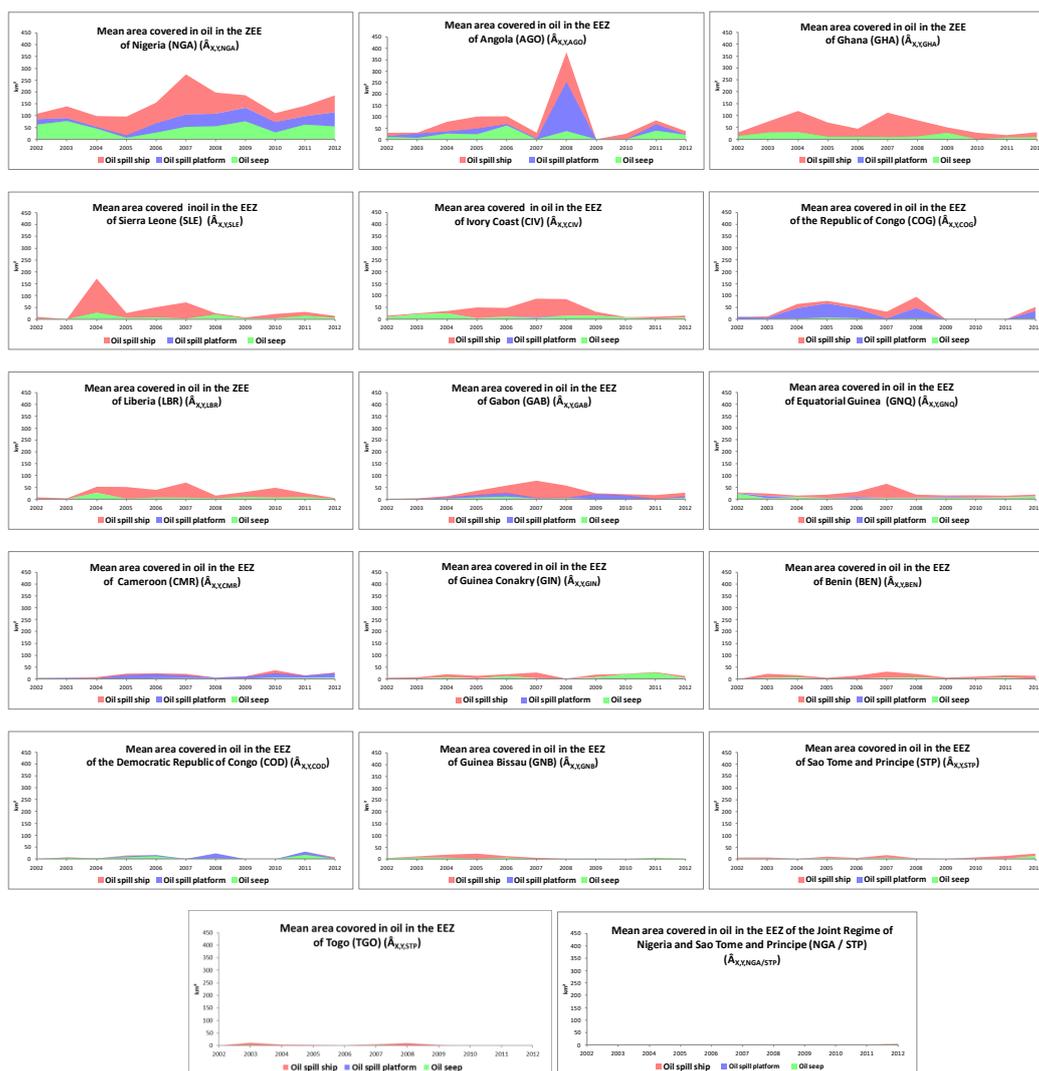
262   *fig. 12 Mean area covered in oil by EEZ of countries per year (Â$_{X,Y,EEZ}$).*

263 **5.3. Mean fraction covered by oil by EEZ ($P_{X,Y,EEZ}$)**

264 The fig. 13 shows the mean fraction covered by oil by EEZ of countries between 2002 and 2012. The fig. 14 shows the mean fraction

265 covered by oil by EEZ of countries by year.

266 The country mean fraction covered by oil which divides the mean area covered in oil by the country EEZ area (eq.7) gives an idea of the

267 mean probability to be covered by oil by EEZ. Thus, the biggest the mean fraction, the more the area is able to be covered by. One may see

268 that the probability that an oil spill occur is high for the Republic of Congo, Cameroon and Nigeria while the probability that an oil seep

269 occur is high for the Democratic Republic of the Cong, Nigeria and Cameroon.
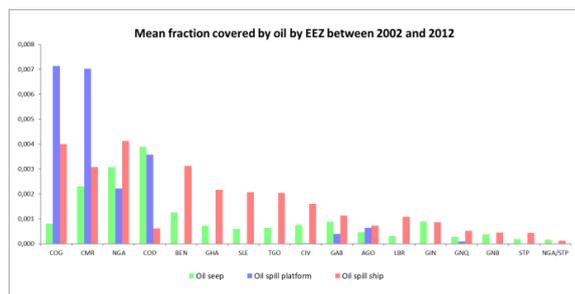
fig. 13 - Mean fraction covered by spilled oil by EEZ between 2002 and 2012.
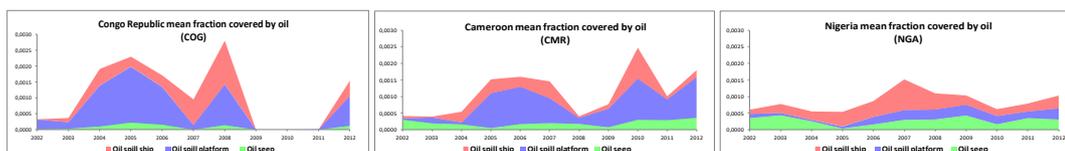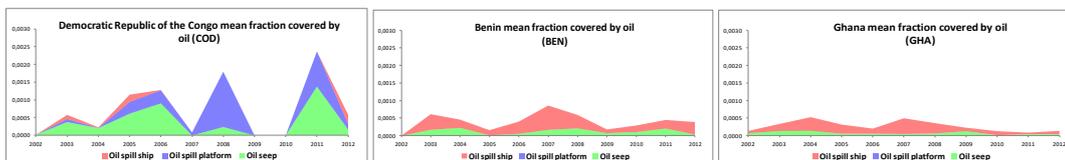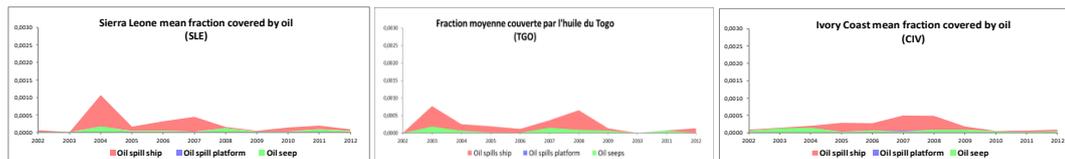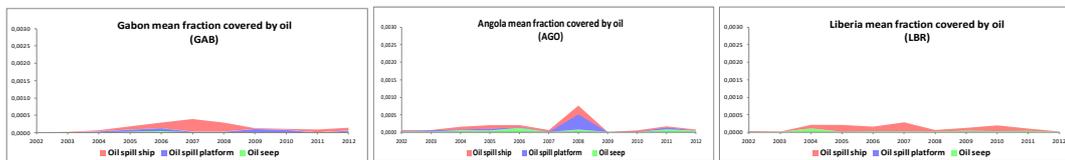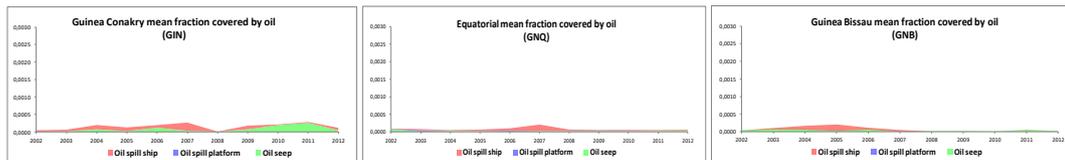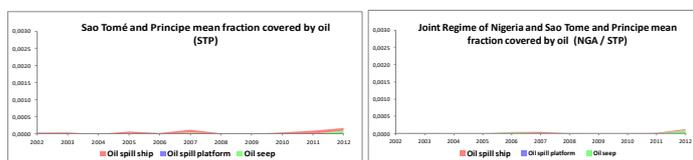
fig. 14 - Mean fraction covered by oil by EEZ by year.

6. Data availability

280   All the Envisat ASAR images (2002-2012) used in this study are available at ESA website https://eocat.esa.int/sec/#data-services-area.

281 The spatial distribution of the oil slicks in the Gulf of Guinea between 2002 and 2012 is available at ZENODO:

282 https://doi.org/10.5281/zenodo.6470470 (Najoui, 2022).

7. Conclusion and perspectives

284   An unprecedented database of oil spills has been generated over the EEZ of the Gulf of Guinea using the 11 years of acquisitions of SAR

285 images at C-band by ASAR in wide-swat mode (150 m of spatial resolution) contained in the archive of the Envisat mission. This database

286 has been achieved using a manual approach. The present study shows that all of the countries EEZ are sites of natural oil seepages due to the

287 extensive geological context of the Gulf of Guinea. It shows also that oil spills from ships are well correlated to the shipping routes along the

288 coasts of the 17 EEZ of the Gulf of Guinea while oil spills coming from oil platforms are concentrated along the coasts of oil-producing

289 countries like Nigeria, Republic of Congo, Angola, and Ghana. The temporal analysis during 10 years (2002-2012) shows a decrease in the

290 mean area covered by oil between 2008 and 2009. This decreasing is likely to be due to the post-2008 global economic slowdown.

291   Oil seepages and oil spills monitoring will benefit from Sentinel-1 mission, launched in 2014, owing to its higher spatial resolution (10

292 m), its temporal sampling (5 days), and its longer period of acquisitions (beyond 2032). This dataset will offer more reliable and timely

293 information for emergency and mitigation policies.

Acknowledgments

295   The authors would like to thank the ESA (European Spatial Agency) for providing the SAR scenes used in this study.

REFERENCES

Adelana, S., Adeosun, T., 2011. Environmental pollution and remediation: challenges and management of oil Spillage in the Nigerian coastal areas. Am. J. Sci. Ind. Res. 2, 834–845. https://doi.org/10.5251/ajsir.2011.2.6.834.845

Albakjaji, M., 2010. La pollution de la mer méditerranée par les hydrocarbures liée au trafic maritime.

Alpers, W., Holt, B., Zeng, K., 2017. Oil spill detection by imaging radars: Challenges and pitfalls. Remote Sens. Environ. 201, 133–147. https://doi.org/10.1016/j.rse.2017.09.002

Bagby, S.C., Reddy, C.M., Aeppli, C., Fisher, G.B., Valentine, D.L., 2017. Persistence and biodegradation of oil at the ocean floor following *Deepwater Horizon*. Proc. Natl. Acad. Sci. 114, E9–E18. https://doi.org/10.1073/pnas.1610110114

Brekke, C., Solberg, A.H.S., 2008. Classifiers and Confidence Estimation for Oil Spill Detection in ENVISAT ASAR Images. IEEE Geosci. Remote Sens. Lett. 5, 65–69. https://doi.org/10.1109/LGRS.2007.907174

Brekke, C., Solberg, A.H.S., 2005. Oil spill detection by satellite remote sensing. Remote Sens. Environ. 95, 1–13. https://doi.org/10.1016/j.rse.2004.11.015

Caruso, M., Migliaccio, M., Hargrove, J., Garcia-Pineda, O., Graber, H., 2013. Oil Spills and Slicks Imaged by Synthetic Aperture Radar. Oceanography 26. https://doi.org/10.5670/oceanog.2013.34

Chalghmi, H., 2015. Etude de la pollution marine par les hydrocarbures et caractérisation de leurs effets biochimiques et moléculaires sur la palourde de Ruditapes sp.

Del Frate, F., Petrocchi, A., Lichtenegger, J., Calabresi, G., 2000. Neural networks for oil spill detection using ERS-SAR data. IEEE Trans. Geosci. Remote Sens. 38, 2282–2287. https://doi.org/10.1109/36.868885

Espedal, H.A., 1999. Satellite SAR oil spill detection using wind history information. Int. J. Remote Sens. 20, 49–65. https://doi.org/10.1080/014311699213596

Favennec, J.-P., Copinschi, P., Cavatorta, T., Esen, F., 2003. Les nouveaux enjeux pétroliers en Afrique. Polit. Afr. 89, 127.

317   https://doi.org/10.3917/polaf.089.0127

318   Fingas, M., Brown, C., 2017. A Review of Oil Spill Remote Sensing. Sensors 18, 91. https://doi.org/10.3390/s18010091

319   Fiscella, B., Giancaspro, A., Nirchio, F., Pavese, P., Trivero, P., 2000. Oil spill detection using marine SAR images. Int. J. Remote Sens. 21,
320   3561–3566. https://doi.org/10.1080/014311600750037589

321   Fuhrer, M., 2012. Transport maritime de produits chimiques liquides et flottants : etude experimentale du rejet accidentel sous-marin suite a
322   un naufrage.

323   Gade, M., Alpers, W., Hühnerfuss, H., Masuko, H., Kobayashi, T., 1998. Imaging of biogenic and anthropogenic ocean surface films by the
324   multifrequency/multipolarization SIR-C/X-SAR. J. Geophys. Res. Oceans 103, 18851–18866. https://doi.org/10.1029/97JC01915

325   Garcia-Pineda, O., MacDonald, I., Zimmer, B., 2008. Synthetic Aperture Radar Image Processing using the Supervised Textural-Neural
326   Network Classification Algorithm, in: IGARSS 2008 - 2008 IEEE International Geoscience and Remote Sensing Symposium.
327   Presented at the IGARSS 2008 - BP IEEE International Geoscience and Remote Sensing Symposium, IEEE, Boston, MA,
328   USA, p. IV-1265-IV–1268. https://doi.org/10.1109/IGARSS.2008.4779960

329   Jackson, C.R., Apel, J.R., United States (Eds.), 2004. Synthetic aperture radar: marine user's manual. U.S. Dept. of Commerce : National
330   Oceanic and Atmospheric Administration, Washington, D.C.

331   Jafarzadeh, H., Mahdianpari, M., Homayouni, S., Mohammadimanesh, F., Dabboor, M., 2021. Oil spill detection from Synthetic Aperture
332   Radar Earth observations: a meta-analysis and comprehensive review. GIScience Remote Sens. 58, 1022–1051.
333   https://doi.org/10.1080/15481603.2021.1952542

334   Jatiault, R., Dhont, D., Loncke, L., Dubucq, D., 2017. Monitoring of natural oil seepage in the Lower Congo Basin using SAR observations.
335   Remote Sens. Environ. 191, 258–272. https://doi.org/10.1016/j.rse.2017.01.031

336   Johannessen, O.M., Sandven, S., Jenkins, A.D., Durand, D., Pettersson, L.H., Espedal, H., Evensen, G., Hamre, T., 2000. Satellite earth
337   observation in operational oceanography. Coast. Eng. 41, 155–176. https://doi.org/10.1016/S0378-3839(00)00030-2

338   Kanaa, T.F.N., Tonye, E., Mercier, G., Onana, V.P., Ngono, J.M., Frison, P.L., Rudant, J.P., Garello, R., 2003. Detection of oil slick
339   signatures in SAR images by fusion of hysteresis thresholding responses, in: IGARSS 2003. 2003 IEEE International Geoscience
340   and Remote Sensing Symposium. Proceedings (IEEE Cat. No.03CH37477). Presented at the IGARSS 2003. 2003 IEEE
341   International Geoscience and Remote Sensing Symposium., IEEE, Toulouse, France, pp. 2750–2752.
342   https://doi.org/10.1109/IGARSS.2003.1294573

343   Khanna, S., Santos, M., Ustin, S., Shapiro, K., Haverkamp, P., Lay, M., 2018. Comparing the Potential of Multispectral and Hyperspectral
344   Data for Monitoring Oil Spill Impact. Sensors 18, 558. https://doi.org/10.3390/s18020558

345   Kubat, M., Holte, R.C., Matwin, S., 1998. Machine Learning for the Detection of Oil Spills in Satellite Radar Images. Mach. Learn. 30, 195–
346   215. https://doi.org/10.1023/A:1007452223027

347   Langangen, Ø., Olsen, E., Stige, L.C., Ohlberger, J., Yaragina, N.A., Vikebø, F.B., Bogstad, B., Stenseth, N.C., Hjermann, D.Ø., 2017. The
348   effects of oil spills on marine fish: Implications of spatial variation in natural mortality. Mar. Pollut. Bull. 119, 102–109.
349   https://doi.org/10.1016/j.marpolbul.2017.03.037

350   Lawrence, S.R., Munday, S., Bray, R., 2002. Regional geology and geophysics of the eastern Gulf of Guinea (Niger Delta to Rio Muni).
351   Lead. Edge 21, 1112–1117. https://doi.org/10.1190/1.1523752

352   Leifer, I., Lehr, W.J., Simecek-Beatty, D., Bradley, E., Clark, R., Dennison, P., Hu, Y., Matheson, S., Jones, C.E., Holt, B., Reif, M.,
353   Roberts, D.A., Svejkovsky, J., Swayze, G., Wozencraft, J., 2012. State of the art satellite and airborne marine oil spill remote
354   sensing: Application to the BP Deepwater Horizon oil spill. Remote Sens. Environ. 124, 185–209.
355   https://doi.org/10.1016/j.rse.2012.03.024

356   Li, Y., Hu, C., Quigg, A., Gao, H., 2019. Potential influence of the Deepwater Horizon oil spill on phytoplankton primary productivity in the
357   northern Gulf of Mexico. Environ. Res. Lett. 14, 094018. https://doi.org/10.1088/1748-9326/ab3735

358   Li, Z., Johnson, W., 2019. An Improved Method to Estimate the Probability of Oil Spill Contact to Environmental Resources in the Gulf of
359   Mexico. J. Mar. Sci. Eng. 7, 41. https://doi.org/10.3390/jmse7020041

360   Liu, A.K., Peng, C.Y., Chang, S.Y.-S., 1997. Wavelet analysis of satellite images for coastal watch. IEEE J. Ocean. Eng. 22, 9–17.
361   https://doi.org/10.1109/48.557535

362   Louet, J., Bruzzi, S., 1999. ENVISAT mission and system, in: IEEE 1999 International Geoscience and Remote Sensing Symposium.
363   IGARSS'99 (Cat. No.99CH36293). Presented at the IEEE 1999 International Geoscience and Remote Sensing Symposium.
364   IGARSS'99, IEEE, Hamburg, Germany, pp. 1680–1682. https://doi.org/10.1109/IGARSS.1999.772059

365   MacDonald, I.R., Garcia-Pineda, O., Beet, A., Daneshgar Asl, S., Feng, L., Graettinger, G., French-McCay, D., Holmes, J., Hu, C., Huffer,
366   F., Leifer, I., Muller-Karger, F., Solow, A., Silva, M., Swayze, G., 2015. Natural and unnatural oil slicks in the G ulf of M exico.
367   J. Geophys. Res. Oceans 120, 8364–8380. https://doi.org/10.1002/2015JC011062

368   Marghany, M., 2015. Automatic detection of oil spills in the Gulf of Mexico from RADARSAT-2 SAR satellite data. Environ. Earth Sci. 74,
369   5935–5947. https://doi.org/10.1007/s12665-015-4617-y

370   Mercier, G., Girard-Ardhuin, F., 2006. Partially Supervised Oil-Slick Detection by SAR Imagery Using Kernel Expansion. IEEE Trans.
371   Geosci. Remote Sens. 44, 2839–2846. https://doi.org/10.1109/TGRS.2006.881078

372   Mfewou, A., Tchekote, H., Lemouogue, J., 2018. Frontières Et Dynamiques Socio-Spatiales En Afrique : Une Analyse À Partir Des
373   Frontières Sud- Camerounaises. Eur. Sci. J. ESJ 14, 285. https://doi.org/10.19044/esj.2018.v14n5p285

374   Mikidadu, M., 2018. Oil Production and Economic Growth in Angola. Int. J. Energy Econ. Policy 8, 127–131.

375   Miranda, N., Rosich, B., Meadows, P.J., Haria, K., Small, D., Schubert, A., Lavalle, M., Collard, F., Johnsen, H., Monti-Guarnieri, A.,
376   D'Aria, D., 2013. The Envisat ASAR mission: A look back at 10 years of operation. https://doi.org/10.5167/UZH-96146

377   NAE-NRC, 2012. Macondo Well Deepwater Horizon Blowout: Lessons for Improving Offshore Drilling Safety. National Academies Press,
378   Washington, D.C. https://doi.org/10.17226/13273

379   Najoui, Z., 2022. Spatial distribution of oil slicks in the Gulf of Guinea between 2002 and 2012. Zenodo.
380   https://doi.org/10.5281/ZENODO.6470470

381   Najoui, Z., 2017. Prétraitement optimal des images radar et modélisation des dérives de nappes d'hydrocarbures pour l'aide à la photo-
382   interprétation en exploration pétrolière et surveillance environnementale.

383   Najoui, Z., Riazanoff, S., Deffontaines, B., Xavier, J.-P., 2018a. Estimated location of the seafloor sources of marine natural oil seeps from
384   sea surface outbreaks: A new "source path procedure" applied to the northern Gulf of Mexico. Mar. Pet. Geol. 91, 190–201.
385   https://doi.org/10.1016/j.marpetgeo.2017.12.035

386   Najoui, Z., Riazanoff, S., Deffontaines, B., Xavier, J.-P., 2018b. A Statistical Approach to Preprocess and Enhance C-Band SAR Images in
387   Order to Detect Automatically Marine Oil Slicks. IEEE Trans. Geosci. Remote Sens. 56, 2554–2564.
388   https://doi.org/10.1109/TGRS.2017.2760516

389   Ngodi, E., 2005. Gestion des ressources pétrolières et développement en Afrique.

390   Okafor-Yarwood, I., 2018. The effects of oil pollution on the marine environment in the Gulf of Guinea—the Bonga Oil Field example.
391   Transnatl. Leg. Theory 9, 254–271. https://doi.org/10.1080/20414005.2018.1562287

392   Ovadia, J.S., 2016. The petro-developmental state in Africa: making oil work in Angola, Nigeria and the Gulf of Guinea. Hurst & Company,
393   London.

394   Pinkston, F.W.M., Flemings, P.B., 2019. Overpressure at the Macondo Well and its impact on the Deepwater Horizon blowout. Sci. Rep. 9,
395   7047. https://doi.org/10.1038/s41598-019-42496-0

396   Reuscher, M.G., Baguley, J.G., Montagna, P.A., 2020. The expanded footprint of the Deepwater Horizon oil spill in the Gulf of Mexico
397   deep-sea benthos. PLOS ONE 15, e0235167. https://doi.org/10.1371/journal.pone.0235167

398   Scheren, P.A., Ibe, A.C., Janssen, F.J., Lemmens, A.M., 2002. Environmental pollution in the Gulf of Guinea – a regional approach. Mar.
399   Pollut. Bull. 44, 633–641. https://doi.org/10.1016/S0025-326X(01)00305-8

400   Shu, Y., Li, J., Yousif, H., Gomes, G., 2010. Dark-spot detection from SAR intensity imagery with spatial density thresholding for oil-spill
401   monitoring. Remote Sens. Environ. 114, 2026–2035. https://doi.org/10.1016/j.rse.2010.04.009

402   Solberg, A.H.S., Storvik, G., Solberg, R., Volden, E., 1999. Automatic detection of oil spills in ERS SAR images. IEEE Trans. Geosci.
403   Remote Sens. 37, 1916–1924. https://doi.org/10.1109/36.774704

404   Suresh, G., Melsheimer, C., Korber, J.-H., Bohrmann, G., 2015. Automatic Estimation of Oil Seep Locations in Synthetic Aperture Radar
405   Images. IEEE Trans. Geosci. Remote Sens. 53, 4218–4230. https://doi.org/10.1109/TGRS.2015.2393375

406   The ENVISAT Mission and System, n.d.

407   Trivero, P., Biamino, W., 2010. Observing Marine Pollution with Synthetic Aperture Radar, in: Imperatore, P., Riccio, D. (Eds.), Geoscience
408   and Remote Sensing New Achievements. InTech. https://doi.org/10.5772/9106

409   Tull, D.M., 2008. Oil and Politics in the Gulf of Guinea by Ricardo Soares de Oliveira London: Hurst & Co/New York: Columbia University
410   Press, 2007. Pp. 379. £20.00 (pb). J. Mod. Afr. Stud. 46, 692–694. https://doi.org/10.1017/S0022278X08003558

411   Xu, L., Shafiee, M.J., Wong, A., Li, F., Wang, L., Clausi, D., 2015. Oil spill candidate detection from SAR imagery using a thresholding-
412   guided stochastic fully-connected conditional random field model, in: 2015 IEEE Conference on Computer Vision and Pattern
413   Recognition Workshops (CVPRW). Presented at the 2015 IEEE Conference on Computer Vision and Pattern Recognition
414   Workshops (CVPRW), IEEE, Boston, MA, USA, pp. 79–86. https://doi.org/10.1109/CVPRW.2015.7301386

415   Yaghmour, F., Els, J., Maio, E., Whittington-Jones, B., Samara, F., El Sayed, Y., Ploeg, R., Alzaabi, A., Philip, S., Budd, J., Mupandawana,
416   M., 2022. Oil spill causes mass mortality of sea snakes in the Gulf of Oman. Sci. Total Environ. 825, 154072.
417   https://doi.org/10.1016/j.scitotenv.2022.154072

418   Zhang, Y., Li, Y., Lin, H., 2014. Oil-Spill Pollution Remote Sensing by Synthetic Aperture Radar, in: Marghany, M. (Ed.), Advanced
419   Geoscience Remote Sensing. InTech. https://doi.org/10.5772/57477

420